

InAs/GaAs square nanomesas: Multimillion-atom molecular dynamics simulations on parallel computers

Xiaotao Su, Rajiv K. Kalia, Aiichiro Nakano, and Priya Vashishta^{a)}

Collaboratory for Advanced Computing and Simulations, Department of Materials Science and Engineering, Department of Physics, and Department of Computer Science, University of Southern California, Los Angeles, California 90089

Anupam Madhukar

Photonic Materials and Devices Laboratory, Departments of Materials Science and Physics, University of Southern California, Los Angeles, California 90089

(Received 18 November 2002; accepted 23 July 2003)

A model potential for GaAs(100) and InAs(100) surface atoms is developed and surface reconstructions on GaAs(100) and InAs(100) are studied with the conjugate gradient (CG) method. Not only does this model reproduce well surface energies for the (100) orientation, it also yields (1×2) dimer lengths in accordance with *ab initio* calculations. Large-scale molecular dynamics (MD) simulations are performed to investigate mechanical stresses in InAs/GaAs nanomesas with $\{101\}$ -type sidewalls. The in-plane lattice constant of InAs layers parallel to the InAs/GaAs(001) interface are found to exceed the InAs bulk value at the twelfth monolayer (ML) and the hydrostatic stresses in InAs layers become tensile above 12 ML. Hence, it is energetically unfavorable for InAs overlayers to exceed 12 ML. This may explain the experimental finding that the growth of flat InAs overlayers is self-limiting to ~ 11 ML on GaAs nanomesas. MD simulations are also used to investigate the lateral size effects on the stress distribution and morphology of InAs/GaAs square nanomesas. Two nanomesas with the same vertical size but different lateral sizes are simulated. While a single stress domain is observed in the InAs overlayer of the smaller mesa, two stress domains are found in the larger mesa. This indicates the existence of a critical lateral size for stress domain formation in accordance with recent experimental findings. It is found that the InAs overlayer in the larger mesa is laterally constrained to the GaAs bulk lattice constant at the interface but vertically relaxed to the InAs bulk lattice constant. Surface energies of GaAs and InAs for the (110) and (111) orientations are also calculated with the MD and CG methods. © 2003 American Institute of Physics. [DOI: 10.1063/1.1609049]

I. INTRODUCTION

Surface energies of GaAs and InAs play a major role in the formation of islands during heteroepitaxy. The molecular beam epitaxial (MBE) growth of InAs on GaAs(100) planar substrates is known to be in the Stranski–Krastanov (SK) mode. During the initial stage of the MBE growth, a wetting layer forms. Further deposition of InAs leads to the formation of three-dimensional InAs islands, since the surface energy of InAs is lower than that of GaAs.

Within the family of zinc-blende III–V semiconductors, a great deal of attention has focused on the GaAs(100) surface due to its importance in electronic and optoelectronic devices. In the past decade, numerous state-of-the-art theoretical and experimental techniques have sought to uncover the atomic structure of GaAs(100).^{1–7} A general consensus has been reached concerning the As-stabilized reconstruction, most notably the 2×4 and $c(4 \times 4)$ phases. In particular, the atomic structure of the As-rich GaAs(100)- $\beta 2(2 \times 4)$ surface has been determined using scanning tunneling microscopy (STM) and first-principles electronic-structure calculations.²

The large (up to $\sim 7\%$) lattice mismatch and associated strain at the InGaAs/GaAs(001) interfaces have recently been utilized to fabricate a number of nanostructures.^{8–14} The strain relief leads to the formation of coherent three-dimensional (3D) island structures on infinite planar substrates with the InAs deposition of ~ 1.6 ML.^{10,11} When these 3D islands are capped by an appropriate material, they provide nanostructures for the study of electronic quantum behavior in zero dimension^{10–15} with applications in electronic and optoelectronic devices.^{15–17} The stress/strain distribution plays an important role in the electronic structure of the resulting quantum dots. This has prompted investigations of stress/strain distributions for capped pyramidal islands on planar substrates based on atomistic simulations,^{18–24} finite element¹⁸ and finite difference¹⁹ implementations of continuum elasticity theory, and analytical models based upon continuum elasticity theory.²⁵ The island structures are formed prior to capping because of the stress, induced due to substrate–overlayer lattice mismatch. This has been systematically examined through a study of the growth of InAs on planar^{9–11} and patterned^{12–14} GaAs(001) substrates. On stripe mesas of sub-100-nm widths on GaAs(001) substrates, deposition of InAs is shown to allow self-assembly of three, two, and single chains of InAs 3D island quantum dots selectively

^{a)}Electronic mail: priyav@usc.edu

on the stripe mesa tops for widths decreasing from 100 nm down to 30 nm.¹⁴ For laterally finite mesas, experiments reveal that when InAs is deposited on $\langle 100 \rangle$ oriented GaAs square mesas of size ≤ 75 nm, the island morphology is suppressed and, instead, a continuous film with flat morphology is observed.¹³ Indeed, the InAs film growth is self-limiting and stops at ~ 11 ML.¹³ In order to understand the self-limiting nature of the InAs film growth on nanomesas, it is important to determine mechanical stresses at the atomistic level and the in-plane lattice constant of InAs layers in the InAs/GaAs square nanomesas.

In recent years, atomistic simulations and first-principle simulations have been widely used to study structural, dynamical, electronic, and mechanical properties of such systems.^{26–35} Using the density-functional approach, Moll *et al.* have calculated the surface energies of GaAs and InAs for the (100), (110), and (111) orientations.^{36,37} They obtain the absolute surface energies for different orientations directly and consistently with the same set of parameters and pseudopotentials without introducing a reference surface. The surface energies are determined *via* total-energy calculations using density-functional theory (DFT) with local-density approximation (LDA) applied to the exchange-correlation functional. Qian *et al.* have carried out total-energy density functional calculations to study the reconstruction of GaAs(100) surfaces as a function of Ga and As surface coverage.³⁸ Equilibrium atomic geometry and energies for Ga- and As-stabilized 1×2 , 2×1 , and 2×2 surfaces consisting of various combinations of dimers and vacancies have been determined.

In this article, we report the molecular dynamics (MD) simulations of InAs/GaAs nanomesas with $\langle 100 \rangle$ oriented square base and $\{101\}$ sidewalls on GaAs(001) substrates. The MD simulations are based on reliable interatomic potentials^{39–41} that can successfully describe a wide range of physical properties of InAs and GaAs. We have investigated the mechanical stresses and in-plane lattice constants of InAs layers parallel to the InAs/GaAs(001) interface in the nanomesas. The MD simulations reveal that on GaAs(001) square nanomesas, InAs overlayer thickness should be self-limited to ~ 12 ML, as experimentally observed. Furthermore, these simulations indicate the existence of a critical lateral size for stress domain formation. Thus, as our simulations reveal, for nanomesas with top lateral sizes greater than 12.4 nm and less than 40.7 nm, the InAs overlayer is laterally constrained to the GaAs bulk lattice constant near the interface but vertically relaxed to the InAs bulk lattice constant.

II. InAs AND GaAs INTERATOMIC POTENTIALS

Our interatomic potentials for GaAs and InAs consist of two- and three-body terms,

$$V = \sum_{i < j} V_{ij}^{(2)}(r_{ij}) + \sum_{i, j < k} V_{jik}^{(3)}(\mathbf{r}_{ij}, \mathbf{r}_{ik}). \quad (1)$$

The two-body terms represent steric repulsion, Coulomb

TABLE I. Two-body potential parameters for each atom type.

Atom type	$\sigma_i(\text{\AA})$	$Z_i(e)$	$\alpha_i(\text{\AA}^3)$
Ga	0.95	0.9418	0
As (of GaAs)	1.498	-0.9418	2
In	1.018	1.1276	0
As (of InAs)	1.605	-1.1276	2

interaction due to charge transfer, charge-induced dipole interaction due to large polarizability of negative ions, and van der Waals interactions:

$$V_{ij}^{(2)}(r_{ij}) = A_{ij} \left(\frac{\sigma_i + \sigma_j}{r_{ij}} \right)^{\eta_{ij}} + \frac{Z_i Z_j}{r_{ij}} e^{-r_{ij}/r_{1s}} - \frac{\alpha_i Z_j^2 + \alpha_j Z_i^2}{2r_{ij}^4} e^{-r_{ij}/r_{4s}} - \frac{W_{ij}}{r_{ij}^6}. \quad (2)$$

The first term represents steric repulsion, which is described by strength prefactors for steric repulsion A_{ij} , ionic radii σ_i and σ_j , and the exponents of steric repulsion η_{ij} . The second term is the Coulomb interaction due to charge transfer and contains the effective atomic charges Z_i and Z_j as parameters. The screening length of the Coulomb interaction, r_{1s} , is set to 5.0 \AA . The third term corresponds to the charge dipole interaction due to large polarizability of negative ions. The screening length for charge-dipole interactions, r_{4s} , is set to 3.75 \AA . The last term is the induced dipole-dipole interaction, containing the van der Waals strengths W_{ij} . The values of the two-body parameters are listed in Tables I and II. The two-body cutoff length r_c is set to 7.5 \AA . In order to make the potentials and forces continuous at the value of r_c , the following equation is employed:

$$V_{ij}(r_{ij}) = V_{ij}(r_{ij}) - V_{ij}(r_c) - V'_{ij}(r_c)(r - r_c). \quad (3)$$

Covalent effects are represented by three-body bond-bending and bond-stretching terms. The three-body term $V_{jik}^{(3)}$ includes bond angles and has the form:

$$V_{jik}^{(3)}(\mathbf{r}_{ij}, \mathbf{r}_{ik}) = B_{jik} \exp \left(\frac{l}{r_{ij} - r_0} + \frac{l}{r_{ik} - r_0} \right) \times \frac{(\cos \theta_{jik} - \cos \bar{\theta}_{jik})^2}{1 + C_{jik}(\cos \theta_{jik} - \cos \bar{\theta}_{jik})^2} \times \Theta(r_0 - r_{ij}) \Theta(r_0 - r_{ik}), \quad (4)$$

where B_{jik} is the strength of the interaction, $\bar{\theta}_{jik}$ is a constant, θ_{jik} is the angle formed by \mathbf{r}_{ij} and \mathbf{r}_{ik} , and $\Theta(r_0$

TABLE II. Two-body potential parameters for each atom pair type.

Atom pair type	$A_{ij}(10^{-19} \text{ J})$	η_{ij}	$W_{ij}(10^{-18} \text{ J } \text{\AA}^6)$
Ga–Ga	16.4984	7	0
Ga–As	2.0623	9	58.916
As–As (GaAs)	2.0623	7	0
In–In	5.3872	7	0
In–As	0.6734	9	0
As–As (InAs)	0.6734	7	0

TABLE III. Three-body potential parameters for each atom triplet.

Atom triplet	$B_{jik}(10^{-19} \text{ J})$	C_{jik}	$\bar{\theta}_{jik}(\text{deg})$
As–Ga–As	7.9	20	109.47122
Ga–As–Ga	7.9	20	109.47122
As–In–As	1.3	4	109.47122
In–As–In	1.3	4	109.47122

$-r_{ij})\Theta(r_0-r_{ik})$ are step functions. The three-body cutoff length r_0 and the characteristic length l are set to 3.8 and 1 Å, respectively. The parameters used for three-body potentials are listed in Table III.

The adjustable parameters in Eqs. (2) and (4) are determined so that results from a set of experimental data and first-principle electronic-structure calculations are reproduced. MD simulation results, based on our potentials, agree well with the experimental crystalline lattice constants, cohesive energies, elastic constants, surface energies,^{36,37} high-pressure structural transitions,⁴² phonon density of states, and neutron-scattering data for liquid and amorphous structures.⁴¹

In the InAs/GaAs nanomesas, atoms at the InAs/GaAs interface reside in a mixed environment of InAs and GaAs. For these atoms, we have developed a scheme that combines interatomic potentials of binary materials (InAs and GaAs) in such a way that the resulting potential depends on the local chemical composition. In such a system involving Ga, In, and As, we use an environment-dependent linear interpolation scheme to combine the interatomic potentials for GaAs and InAs.^{43,44} Such an interpolation scheme can be generally applied to systems containing an interface between two bulk materials. In this adaptive scheme, As atoms are classified into different types according to the number of Ga and In neighbor atoms:

(i) For the two different cations (Ga and In), the two-body potential between them is the average of the cation–cation interaction potentials in the pure compounds (GaAs and InAs),

$$V_{\text{Ga-In}}^{(2)} = \frac{V_{\text{Ga-Ga}}^{(2)} + V_{\text{In-In}}^{(2)}}{2}. \quad (5)$$

(ii) The first neighbor shell of each cation is As, whereas the first neighbor of As is either Ga or In. Therefore, we have five different neighbor configurations for As and, consequently, five different types of As in the alloy. The two-body interaction potential between As interpolates the potentials in the pure compounds. The As–As interaction potential is interpolated as follows:

$$V_{\text{As}_x\text{-As}_y}^{(2)} = \frac{2-x-y}{2} V_{\text{As}_0\text{-As}_0}^{(2)} + \frac{x+y}{2} V_{\text{As}_1\text{-As}_1}^{(2)}, \quad (6)$$

where $x, y = n/4$ ($n = 0, \dots, 4$), and n is the number of In neighbors around the As atom. There are five different As types (corresponding to $n = 0, \dots, 4$): (1) As with four Ga neighbors, i.e., As in pure GaAs; (2) As with three Ga neighbors and one In neighbor; (3) As with two Ga neighbors and

two In neighbors; (4) As with one Ga neighbor and three In neighbors; and (5) As with four In neighbors, i.e., As in pure InAs.

(iii) The three-body interaction potential Ga–As–In is the average of the three-body interactions in the pure compounds:

$$V_{\text{Ga-As-In}}^{(3)} = \frac{V_{\text{Ga-As-Ga}}^{(3)} + V_{\text{In-As-In}}^{(3)}}{2}. \quad (7)$$

All the remaining two- and three-body interactions are the same as those in the pure compounds.

III. SURFACE ENERGIES OF GaAs AND InAs SURFACES

We have used MD simulations to calculate surface energies for the (100), (110), and (111) orientations of GaAs and InAs. Two sets of calculations are performed: (1) those based on interatomic potentials of the form of Eq. (1), without modeling surface atoms, i.e., the surface atoms are treated as bulk atoms and surface reconstruction is not taken into account; and (2) calculations based on a model interaction for GaAs(100) and InAs(100) surfaces. We note that, although the interaction potentials we use are highly accurate, it would be too much to expect that these interatomic potentials, developed to reproduce the bulk properties of the materials, will also provide an absolutely accurate description of surface reconstructions effects. Therefore, at best, we expect only a qualitative agreement in surface energies description. However, this simple treatment may provide valuable guidance in the modeling of GaAs and InAs surface atoms. In the next section, we will present results based on the interaction model for GaAs(100) and InAs(100) surfaces.

In the calculation of GaAs(100) surface energy, we start with a slab supercell of size $28.266 \text{ \AA} \times 28.266 \text{ \AA} \times 28.266 \text{ \AA}$ (i.e., $5 \times 5 \times 5$ unit cells) containing 1000 atoms.⁴⁵ The z axis is (001) oriented and a 10 Å gap is inserted in the z direction to create two GaAs(100) surfaces, which are As and Ga terminated, respectively. Periodic boundary conditions are applied only in the x and y directions, which are [100] and [010], respectively. The equations of motion are integrated using a reversible symplectic algorithm⁴⁶ with a time step $\Delta t = 2.0$ fs. The system is first quenched to 0 K every $10\Delta t$ for $200\Delta t$, i.e., the velocities of all the atoms are set to zero every $10\Delta t$. Subsequently, we quench the system with a factor of 0.3 every $10\Delta t$ for $200\Delta t$, i.e., the velocities of all atoms are multiplied by a factor of 0.3 every $10\Delta t$. Then, the system is quenched with

TABLE IV. MD, CG, *ab initio* calculations, and experiment results for GaAs surface energies of the (100), (110), and (111) orientations.

Orientations	(110)	(100)	(111)
MD ^a	0.621 J/m ²	1.692 J/m ²	0.722 J/m ²
CG ^a	0.621 J/m ²	1.692 J/m ²	0.722 J/m ²
<i>Ab initio</i> ^b	0.83 J/m ²	~1.0 J/m ²	~0.96 J/m ²
Experiment ^c	$0.87 \pm 0.1 \text{ J/m}^2$	N/A	N/A

^aWithout modeling surface atoms.^bFrom Ref. 36.^cFrom Ref. 47.

TABLE V. MD, CG, and *ab initio* calculations for InAs surface energies of the (100), (110), and (111) orientations.

Orientations	(110)	(100)	(111)
MD ^a	0.333 J/m ²	1.126 J/m ²	0.464 J/m ²
CG ^a	0.333 J/m ²	1.125 J/m ²	0.463 J/m ²
<i>Ab initio</i> ^b	0.656 J/m ²	~0.704 J/m ²	~0.672 J/m ²

^aWithout modeling surface atoms.

^bFrom Ref. 37.

a factor of 0.6 every $10\Delta t$ for $200\Delta t$, followed by a quenching with a factor of 0.9 every $10\Delta t$ for $400\Delta t$. Finally, the system is allowed to relax at system temperatures around 0.0001 K for time period of $13000\Delta t$. At this point, the system is in an equilibrium state and we calculate the energy $\langle E \rangle$, which corresponds to the GaAs cube with two GaAs(100) surfaces.

The GaAs(100) surface energy is calculated from

$$\gamma = \frac{\langle E \rangle - \langle E \rangle_{\text{bulk}}}{2A}, \quad (8)$$

where $\langle E \rangle_{\text{bulk}}$ is the GaAs bulk energy and A is the surface area. We have also used the conjugate gradient (CG) method to calculate the energy $\langle E \rangle$ in Eq. (8) for the same setup as in the MD simulation. The results are given in Table IV.^{36,47} In this article, we have used the same numerical procedure with that employed to obtain the results of Table IV, for all the MD simulations and CG calculations.

The MD results of GaAs surface energies for the GaAs(110) and GaAs(111) orientations are reasonable compared with the *ab initio* calculations and fracture experiments, having an approximately 25% difference. It turns out that the GaAs(110) surface is stoichiometric, i.e., there are equal numbers of Ga and As atoms on the surface and it is the cleavage plane. Such a cleavage surface does not reconstruct, and only a relaxation of surface atomic positions within the (1×1) surface unit cell is observed. On the other hand, the MD results for GaAs(100) surface energy differ substantially from the *ab initio* calculation (~63% higher). The reason is that the (100) surface is polar, i.e., the planes parallel to the surface consist of either Ga or As atoms. As a result, the (001) surface displays various reconstructions, not describable by our model potentials, if the surface atoms are not treated in a special way (See Sec. IV).

We have also calculated InAs surface energies for the (100), (110), and (111) orientations using MD simulations and the CG method. These results are shown in Table V. From Table V we find that the MD results for InAs surface

TABLE VI. Two-body potential parameters for each atom type on the surface.

Atom type	$\sigma_i(\text{\AA})$	$Z_i(e)$	$\alpha_i(\text{\AA}^3)$
Ga2	1.1 (0.95) ^a	0.6660	0
As2 (of GaAs)	1.498	-0.6660	2
In2	1.36	0.79733	0
As2 (of InAs)	1.87	-0.79733	2

^aFor the interaction between two Ga2 atoms only, use 1.1, otherwise use 0.95.

TABLE VII. Two-body potential parameters for each atom pair type on the surface.

Atom pair type	$A_{ij}(10^{-19} \text{ J})$	η_{ij}	$W_{ij}(10^{-18} \text{ J } \text{\AA}^6)$
Ga2-Ga2	16.4984	7	211
Ga2-As1	2.0623	9	70
Ga1-As2	2.0623	9	65
As2-As2 (GaAs)	2.0623	7	220
In2-In2	5.3872	7	305
In2-As1	0.6734	9	65
In1-As2	0.6734	9	45
As2-As2 (InAs)	0.6734	7	335

energies agree well with those based on the CG method. This is as expected, since the same description of interatomic interactions has been used in both methods. It is also found that the MD results of InAs surface energies for the (110) and (111) orientations are reasonable compared with *ab initio* calculations, which is not the case for the (100) surface. The reason for this discrepancy is similar to that for GaAs(100), as discussed in the previous paragraph.

IV. MODEL POTENTIAL FOR GaAs(100) AND InAs(100) SURFACE

Based on *ab initio* calculations and experimental measurements, such as surface energies and dimer lengths, we have developed model potentials for GaAs(100) and InAs(100) surface atoms. Not only do these model potentials reproduce well the surface energies for the (100) orientation, these also yield dimer lengths in accordance with the *ab initio* calculations.

The model for GaAs(100) and InAs(100) surface atoms has four different types of surface atoms: Ga, As of GaAs, and In, As of InAs. These atoms are denoted as: Ga1 for bulk

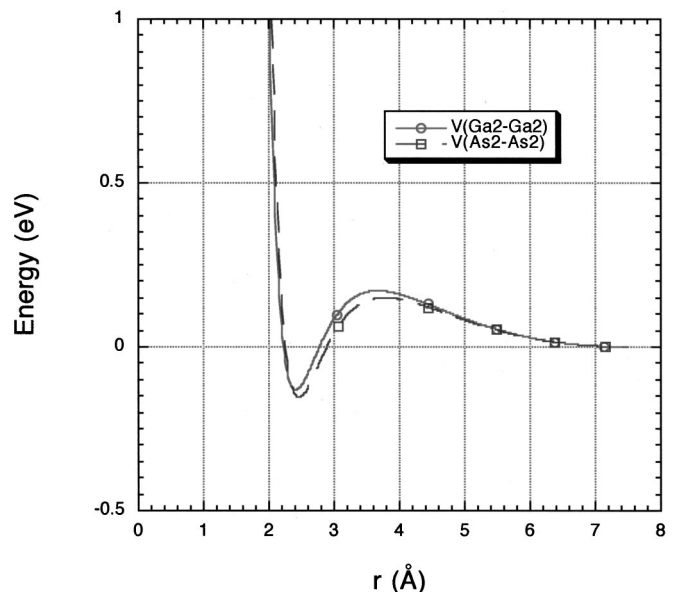


FIG. 1. Two-body interactions between GaAs(100) surface atoms. $V(\text{Ga2-Ga2})$ is the interatomic potential between Ga surface atoms, and $V(\text{As2-As2})$ is the interatomic potential between As of GaAs surface atoms.

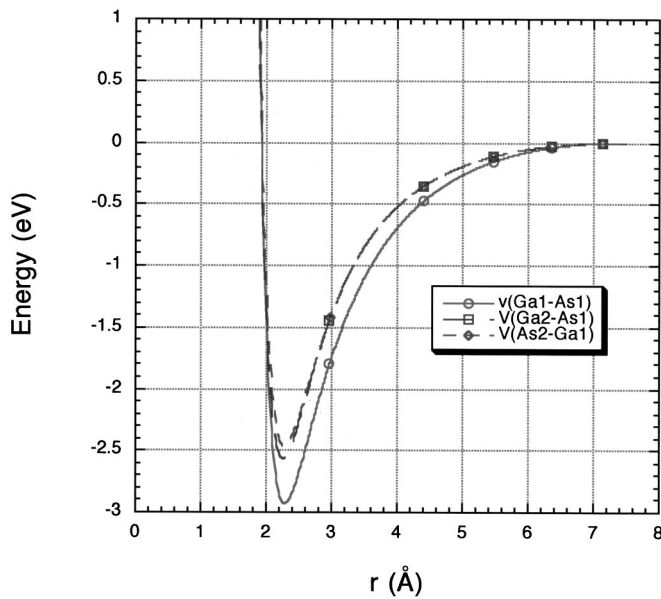


FIG. 2. Two-body interactions between GaAs(100) surface and bulk atoms compared to the two-body interactions between bulk GaAs. $V(\text{Ga1}-\text{As1})$ is the interatomic potential between bulk Ga and As, $V(\text{Ga2}-\text{As1})$ is the interatomic potential between surface Ga and bulk As, and $V(\text{As2}-\text{Ga1})$ is the interatomic potential between surface As of GaAs and bulk Ga.

Ga, Ga2 for surface Ga, As1 for bulk As, As2 for surface As, In1 for bulk In, and In2 for surface In. Each type of surface atom is treated as a new species of atom, different from its bulk counterpart. The two-body interactions for bulk atoms of GaAs and InAs are described in Eq. (2). The two-body interactions between surface atoms, as well as those between surface atoms and bulk atoms, are also in the form of Eq. (2), but with different parameters. These parameters include the effective atomic charges, the ionic radii, and the van der Waals strengths. The effective atomic charges of surface at-

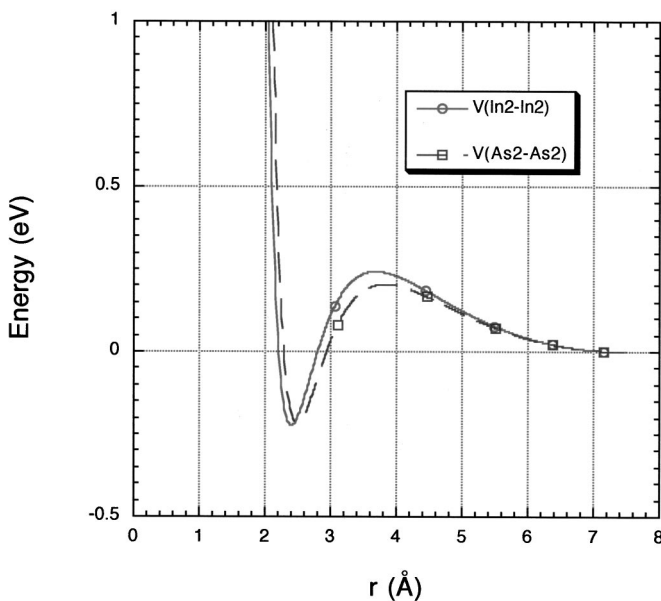


FIG. 3. Two-body interactions between InAs(100) surface atoms. $V(\text{In2}-\text{In2})$ is the interatomic potential between In surface atoms, and $V(\text{As2}-\text{As2})$ is the interatomic potential between As of InAs surface atoms.

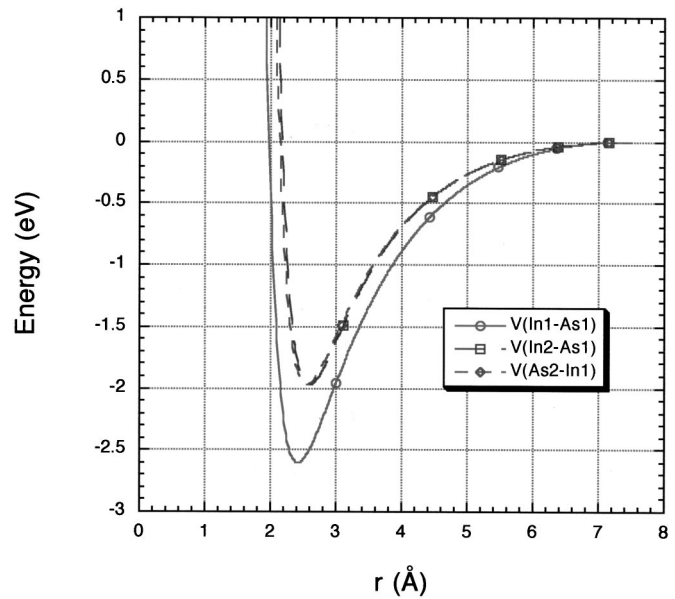


FIG. 4. Two-body interactions between InAs(100) surface and bulk atoms compared to the two-body interactions between bulk InAs. $V(\text{In1}-\text{As1})$ is the interatomic potential between bulk In and As, $V(\text{In2}-\text{As1})$ is the interatomic potential between surface In and bulk As, and $V(\text{As2}-\text{In1})$ is the interatomic potential between surface As of InAs and bulk In.

oms are chosen to be $1/\sqrt{2}$ of that of their bulk counterparts. Other parameters, namely, the ionic radii and the van der Waals strengths, are determined through a trial-and-error process. The values of the two-body parameters for GaAs(100) and InAs(100) surface atoms are listed in Tables VI and VII. As far as three-body interactions are concerned, the surface atoms are like their bulk counterparts, as described in Eq. (4).

Figure 1 shows two-body interactions between GaAs(100) surface atoms. A minimum is found at a distance of ~ 2.4 Å, which is roughly the dimer length. Figure 2 compares the two-body interactions between GaAs(100) surface and bulk atoms and the two-body interactions between bulk atoms in GaAs. We find that the bulk potential is lower than the potential between surface and bulk atoms. This also holds for InAs(100), as shown in Figs. 3 and 4.

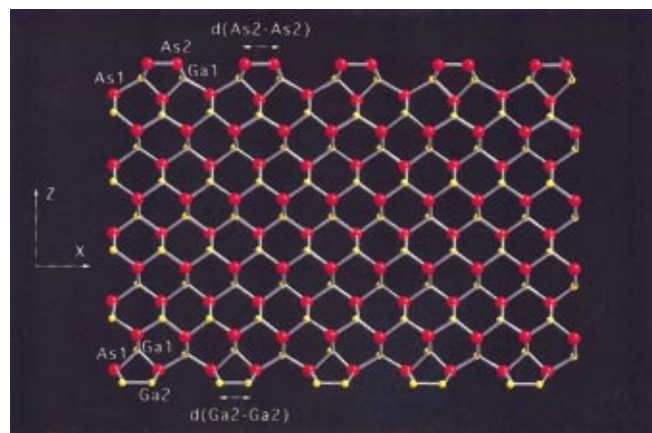


FIG. 5. (Color) As (1×2) and Ga (1×2) dimers on GaAs(100) surfaces.

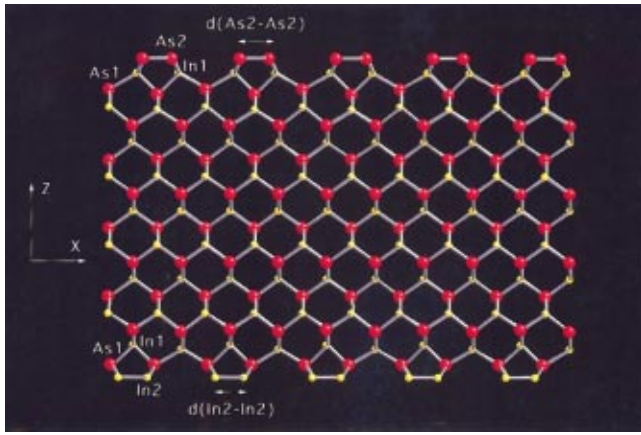


FIG. 6. (Color) As (1×2) and In (1×2) dimers on InAs(100) surfaces.

The model potential for GaAs(100) and InAs(100) surface atoms reproduces well the surface energies. The GaAs(100) surface energy calculated by MD is 1.03 J/m², which is slightly larger than the *ab initio* result of ~1.0 J/m². For InAs(100) surface energy, the MD result is 0.640 J/m², close to the *ab initio* result of ~0.704 J/m². In addition, the model potential yields (1×2) dimer on both the GaAs(100) and InAs(100) surfaces. Figure 5 shows a cross-sectional view of a GaAs slab with (100) oriented surfaces terminated by As and Ga atoms; As(1×2) and Ga(1×2) dimers are observed at the top and bottom, respectively. Similarly, a cross-sectional view of the InAs slab in Fig. 6 shows As(1×2) and In(1×2) dimers at the top and bottom, respectively.

The dimer bond lengths of As and Ga surface atoms on GaAs(100) are listed in Table VIII. The MD simulations yield an As(1×2) dimer bond length of 2.45 Å, which agrees well with the value of 2.51 Å obtained from the *ab initio* calculations (the difference is only 2%). The MD result also agrees well with the *ab initio* calculations for the β2(2×4) and α(2×4) dimer bond lengths, which are 2.50 and 2.45 Å, respectively.

Table VIII also shows that the MD result for the Ga(1×2) dimer agrees well with *ab initio* calculations. The MD simulations yield Ga(1×2) dimer bond lengths of 2.39 Å, which is in good agreement with the value of 2.31 Å obtained from the *ab initio* calculations of the same dimer. The MD result also agrees well with the *ab initio* calculations for the β2(2×4) and α(2×4) dimer bond lengths, which are

TABLE VIII. Dimer bond lengths on GaAs(100) surfaces from *ab initio* calculation, atomistic results based on the model potential for GaAs (100), and the % error.

	$d(\text{As2}-\text{As2})$	$d(\text{Ga2}-\text{Ga2})$
<i>Ab initio</i> ^a (1×2) dimer	2.51 Å	2.31 Å
Atomistic ^b (1×2) dimer	2.45 Å	2.39 Å
Error of atomistic ^b %	-2.4	3.5
<i>Ab initio</i> ^c β2(2×4) dimer	2.50 Å	2.40 Å
<i>Ab initio</i> ^c α(2×4) dimer	2.45 Å	2.50 Å

^aFrom Ref. 38.

^bThe model potential for surface atoms.

^cFrom Ref. 36.

TABLE IX. Bond lengths and angles of As(1×2) and Ga(1×2) dimer on GaAs(100) surfaces from *ab initio* calculations, atomistic results based on the model potential for GaAs (100), and the % error.

	<i>Ab initio</i> ^a (1×2) dimer	Atomistic ^b (1×2) dimer	Error (%)
$d(\text{As2}-\text{Ga1})$	2.40 Å	2.39 Å	-0.4
$\theta(\text{As2}-\text{Ga1}-\text{As1})-1$	101.14°	102.29°	1.1
$\theta(\text{As2}-\text{Ga1}-\text{As1})-2$	118.20°	115.49°	-2.3
$\theta(\text{Ga1}-\text{As2}-\text{Ga1})$	108.87°	113.66°	4.4
$d(\text{Ga2}-\text{As1})$	2.30 Å	2.33 Å	1.3
$\theta(\text{Ga2}-\text{As1}-\text{Ga1})-1$	84.01°	96.49°	15
$\theta(\text{Ga2}-\text{As1}-\text{Ga1})-2$	122.05°	116.79°	-4.3
$\theta(\text{As1}-\text{Ga2}-\text{As1})$	115.60°	118.02°	2.1

^aFrom Ref. 38.

^bThe model potential for surface atoms.

2.40 and 2.50 Å, respectively. The bond lengths and angles for As(1×2) and Ga(1×2) dimers are shown in Table IX. Again, the MD results are close to the *ab initio* calculations. Note that only the two-body interaction parameters of the surface atoms have been fitted according to *ab initio* calculations of surface energies and dimer bond lengths (not including bond angles information), and the three-body interaction parameters have not been changed. So, we can test our model by comparing the bond angles of our MD results with those of *ab initio* calculations, and the difference is at most 15%, as shown in Table IX. For the InAs(100) surface, there are only *ab initio* calculations for the As(1×2) dimer, and they agree well with the MD results; see Table X. Table XI shows the MD results of bond lengths and angles for As(1×2) and In(1×2) dimers on InAs(100) surfaces. Similarly, only the two-body interaction parameters of the surface atoms have been fitted according to *ab initio* calculations, and the three-body interaction parameters are unchanged.

V. FLAT InAs OVERLAYERS ON GaAs SQUARE NANOMESAS

In the following two sections, we report MD simulations of nanomesas with <100> oriented square base and {101}-type sidewalls on GaAs(001) substrates. We have investigated mechanical stresses and the in-plane lattice constant of InAs layers parallel to the InAs/GaAs(001) interface in the nanomesas. Figure 7 shows a schematic of an InAs/GaAs nanomesa with *n* ML InAs overlayer, <100> oriented square base, and {101}-type sidewalls on a GaAs(001) substrate. Periodic boundary conditions are applied to the GaAs substrate of size $L = 474.9$ Å in both *x* and *y* directions. We have tested the convergence with respect to the system size *L*, by per-

TABLE X. Dimer bond lengths of As(1×2) and In(1×2) on InAs(100) surfaces from experiment and atomistic results based on the model potential for InAs(100).

	As2-As2	In2-In2
Atomistic ^a (1×2) dimer	2.44 Å	2.35 Å
Experiment ^b β2(2×4)	2.44 Å, 2.47 Å	N/A

^aThe model potential for surface atoms.

^bFrom Ref. 1. The two values correspond to upper and lower dimer bond lengths, respectively.

TABLE XI. Bond lengths and angles of As(1×2) and In(1×2) dimer on InAs(100) surfaces from atomistic results based on the model potential for InAs(100).

Atomistic ^a (1×2) dimer	
$d(\text{As2}-\text{In1})$	2.63 Å
$\theta(\text{As2}-\text{In1}-\text{As1})-1$	102.75°
$\theta(\text{As2}-\text{In1}-\text{As1})-2$	118.27°
$\theta(\text{In1}-\text{As2}-\text{In1})$	108.79°
$d(\text{In2}-\text{As1})$	2.65 Å
$\theta(\text{In2}-\text{As1}-\text{In1})-1$	101.16°
$\theta(\text{In2}-\text{As1}-\text{In1})-2$	119.42°
$\theta(\text{As1}-\text{In2}-\text{As1})$	107.91°

^aThe model potential for surface atoms.

forming another simulation in which L is increased to 543 Å with all the other dimensions fixed. The in-plane lattice constant in this case differs at most 0.05%, suggesting that the finite-size effect is negligible. The top size of the GaAs mesa is 124.4 Å × 124.4 Å and the system consists of 2,205,157 atoms.

We construct an initial MD configuration of the InAs/GaAs nanomesa with a 16 ML InAs overlayer, in which the lattice constant of InAs is set equal to that of GaAs. The equations of motion are integrated using a reversible symplectic algorithm⁴⁶ with a time step Δt of 2.0 fs. The system is first quenched to 0 K for $10\Delta t$, i.e., the velocities of all atoms are set to zero every Δt . Subsequently, we quench the system with a factor of 0.8 whenever the temperature of the system is higher than 3 K, every $5\Delta t$ for $5000\Delta t$.

At the atomic level, the stress tensor can be determined by computing the interatomic forces arising from interactions between neighboring atoms. In this approach, the stress is assigned to either small regions of space or to individual atoms. However, the stresses are not uniquely defined on the atomistic level because stress is inherently related to the assumption of continuity. In MD simulations, stresses normally

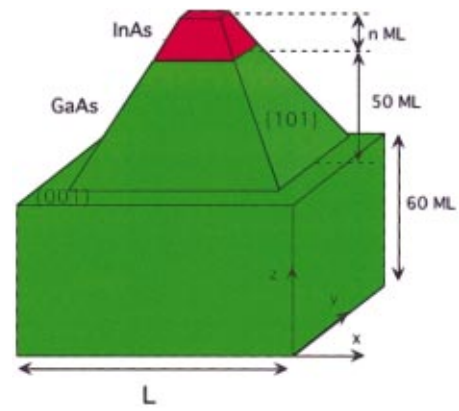


FIG. 7. (Color) Schematic of an InAs/GaAs nanomesa with $\langle 100 \rangle$ oriented square base and $\{101\}$ sidewalls on a GaAs (001) substrate.

need to be calculated over length scales of a few interatomic distances. Also, the symmetry of the stress tensor has to be preserved. Furthermore, the atomistic stress should vanish for systems, which are expected to be under zero stress (for example, an ideal crystal in equilibrium). In our calculations, atomic-level stresses have been defined using the virial approach. Thus, the stress tensor associated with an atom i , $\sigma_{\alpha\beta}^i$, is calculated using

$$\sigma_{\alpha\beta}^i = \frac{1}{\Omega_i} \left\langle \sum_j m_j v_j^\alpha v_j^\beta + \frac{1}{2} \sum_j \sum_k r_{jk}^\alpha f_{jk}^\beta \right\rangle, \quad (9)$$

where $(\alpha, \beta) \equiv (x, y, z)$, m_i and v_i are the mass and velocity of the atom i , f_{ij} is the force acting on atom i due to atom j , r_{ij} is the vector connecting atoms i and j , and Ω_i is the average atomic volume, associated with the atom i . Figure 8 show atomic-level hydrostatic stresses (defined as $[\sigma_{xx} + \sigma_{yy} + \sigma_{zz}]/3$) in the InAs/GaAs nanomesa with a 16 ML InAs overlayer, after quenching for $5000\Delta t$.

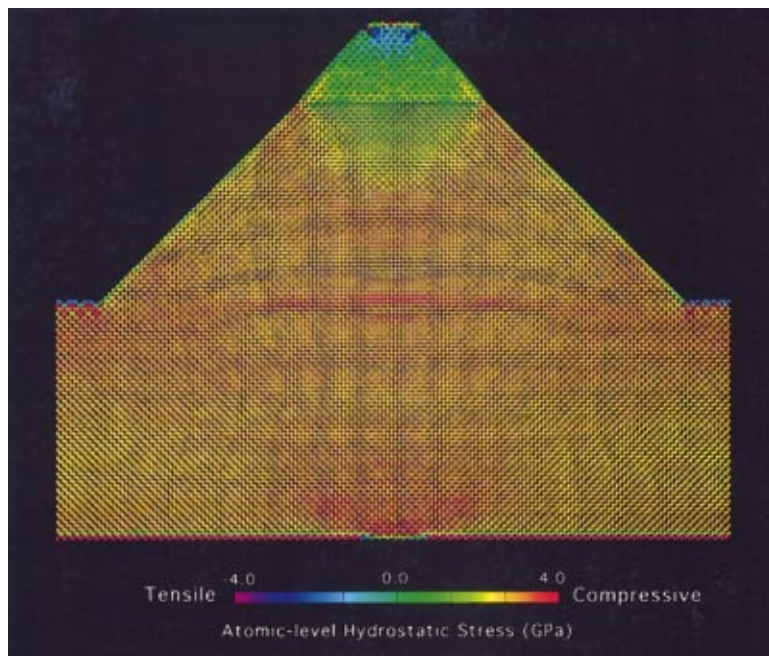


FIG. 8. (Color) Atomic-level hydrostatic stress distribution in an InAs/GaAs square nanomesa with a 16 ML InAs overlayer after being quenched for $5000\Delta t$. Negative pressure means tensile and positive pressure means compressive. Note the presence of cracks at the top of the InAs overlayer.

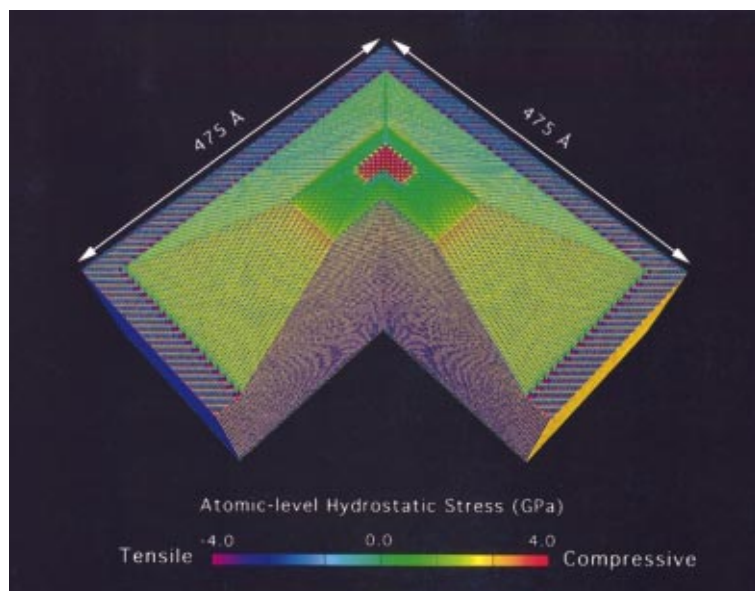


FIG. 9. (Color) Atomic-level hydrostatic stress distribution in an InAs/GaAs square nanomesa with a 12 ML InAs overlayer. Negative pressure means tensile and positive pressure means compressive.

The hydrostatic stress in the InAs layer is found to be tensile above ~ 12 ML after the nanomesa has been quenched for $5000\Delta t$. Cracks develop on top of the nanomesa, due to the tensile stress, see Fig. 8. However, the hydrostatic stress in the InAs layer below ~ 12 ML is still compressive. We are interested in an InAs/GaAs square nanomesa with a 12 ML flat InAs layer, which is the thickness observed experimentally.¹³ So, we remove the top 4 ML of InAs from the 16 ML InAs overlayer, and quench the system to 0 K. Subsequently, we quench the system with a factor of 0.3 whenever the temperature of the system is higher than 0.5 K, every $5\Delta t$ for $500\Delta t$. Then, the system is quenched with a factor of 0.8 whenever the temperature of the system is higher than 0.5 K, every $5\Delta t$ for $29\,500\Delta t$. At this point, the InAs/GaAs nanomesa with a 12 ML InAs overlayer is in a mechanically stable state.

Figure 9 shows atomic-level hydrostatic stresses in the InAs/GaAs nanomesa with a 12 ML InAs overlayer. Due to

the lattice mismatch, a tensile stress well is formed in GaAs immediately below the InAs/GaAs interface. In Fig. 10 we show a cross-sectional view of the atomic stress component σ_{xx} in the InAs/GaAs square nanomesa with a 12 ML InAs overlayer. In the InAs layer, σ_{xx} is found to be compressive and in GaAs near the InAs/GaAs interface, tensile. The in-plane lattice constant of the InAs layer gradually increases with the number of InAs monolayer.

The lattice mismatch between InAs and GaAs, as well as the geometry of the nanomesa, play an important role in the relaxation of the InAs layers. The effect of lattice mismatch can be qualitatively isolated by studying a GaAs square nanomesa of exactly the same geometry as the InAs/GaAs square nanomesa, with the 12 ML InAs overlayer replaced by 12 ML of GaAs. The system is quenched and thermalized by scaling atomic velocities for 35 000 time steps. When the system reaches a mechanically stable state, the in-plane lattice constant of each monolayer of the 12 ML GaAs over-

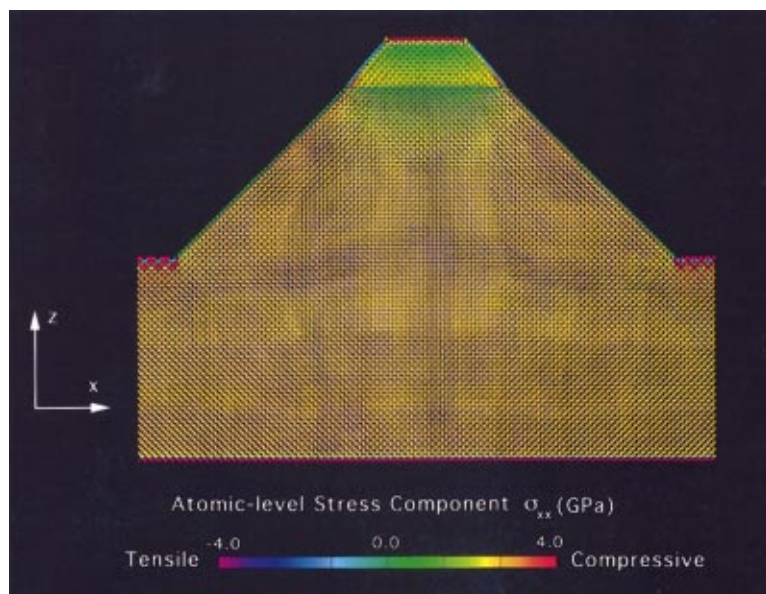


FIG. 10. (Color) Cross-sectional view of the atomic-level stress component σ_{xx} in an InAs/GaAs square nanomesa with a 12 ML InAs overlayer. The figure shows a slice at the center of the nanomesa.

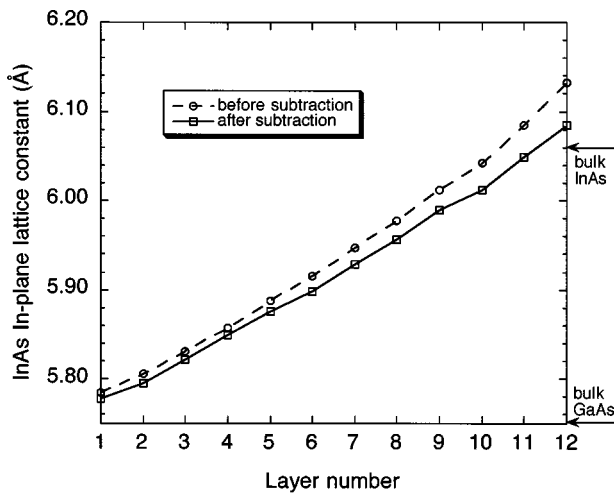


FIG. 11. In-plane lattice constant of each monolayer of the 12 ML InAs overlayer on the InAs/GaAs nanomesa, before and after it is subtracted by the net increase of in-plane lattice constant of the corresponding 12 ML GaAs overlayer on the GaAs nanomesa.

layer in the GaAs square nanomesa is calculated. It is found that the in-plane lattice constant increases monotonically as a function of the layer number, with higher value than the GaAs bulk lattice constant (5.653 Å). The net increase in the in-plane lattice constant of the 12 ML GaAs overlayer with respect to the GaAs bulk value is caused by the geometry of the nanomesa. This net increase is subtracted from the in-plane lattice constant of the corresponding 12 ML InAs overlayer in the InAs/GaAs nanomesa to isolate the effect of lattice mismatch.

In Fig. 11 we show the in-plane lattice constant of each monolayer of the 12 ML InAs overlayer on the InAs/GaAs nanomesa, before and after subtracting the net increase of the in-plane lattice constant of the corresponding 12 ML GaAs overlayer on the GaAs nanomesa. The subtracted in-plane lattice constant of the twelfth InAs monolayer is 6.083 Å, which is slightly larger than the InAs bulk value (6.058 Å). We have also performed similar simulations for InAs/GaAs square nanomesas with 14 and 16 ML InAs overlayers. In these nanomesas, the hydrostatic stresses in InAs layers are tensile above the twelfth monolayer, in contrast to the compressive stresses in the InAs layers below the twelfth monolayer. The hydrostatic stress in the InAs layer plays an important role in the energetic stability of the system, as evidenced by Fig. 8, in which the energetically unstable nanomesa has an overlayer of 16 ML InAs. Cracks are found to develop on top of the nanomesa, due to the tensile stress above ~ 12 ML, after the nanomesa being quenched for $5000\Delta t$. However, in the energetically stable nanomesa that contains an overlayer of 12 ML InAs, as shown in Fig. 9, the topmost InAs layer remains intact and the hydrostatic stress in that layer is compressive. Therefore, the change from compressive to tensile stress may explain the experimental finding that the growth of flat InAs overlayers is self-limiting to ~ 11 ML on GaAs nanomesas.¹³

Recently, continuum elasticity theory has been successfully used to explain and fit atomistic simulation results in strained-layer heteroepitaxial systems.⁴⁸ A hybrid MD/finite-

element simulation approach has been developed to provide atomistic description near the interface and continuum description deep into the substrate.^{49,50} Not only does such a multiscale approach increase the accessible length scales, it also greatly reduces the computational cost.

VI. CRITICAL LATERAL SIZE FOR STRESS DOMAIN FORMATION IN InAs/GaAs SQUARE NANOMESAS

In this section, we investigate the lateral size effects on the stress distribution and morphology of InAs/GaAs square nanomesas with $\{101\}$ -type sidewalls. The simulations involve a larger nanomesa than the one shown in Fig. 7. The larger nanomesa has a size of $L=916$ Å in both x and y directions, with a GaAs mesa top size of 407 Å \times 407 Å. This system consists of 8.5 million atoms. The two nanomesas have the same geometry and the heights of both the GaAs substrate and the mesas are kept the same. In the following, we denote the two nanomesas by their GaAs mesa top size, i.e., the larger mesa is denoted as a “407 Å nanomesa” and the smaller mesa as a “124 Å nanomesa.” Periodic boundary conditions are applied to the 407 Å nanomesa in both x and y directions. The initial configuration of the InAs/GaAs nanomesa is constructed by setting the lattice constant of InAs the same as that of GaAs. The equations of motion are integrated with a reversible symplectic algorithm⁴⁶ using a time step of 2.0 fs. Similar to the quench and relaxation process for the 124 Å nanomesa, the 407 Å nanomesa is quenched and relaxed by scaling atomic velocities for 56 000 time steps. After the system reaches a mechanically stable state, the atomic-level hydrostatic stresses are calculated.

Figure 12 shows these stress in the vertical cross section at the center of the 124 and 407 Å nanomesas. In GaAs immediately below the InAs/GaAs interfaces, tensile stress wells are formed due to the lattice mismatch. Figure 12(a) shows that in the 124 Å nanomesa the hydrostatic stress in the InAs overlayer is compressive (with respect to the InAs bulk lattice constant) and is homogeneous near the interface. However, in the 407 Å nanomesa shown in Fig. 12(b), the hydrostatic stress in the InAs overlayer is inhomogeneous and consists of a highly compressive domain at the center of the InAs overlayer, whereas the peripheral region of the InAs overlayer is less compressive.

Figure 13 shows vertical displacements of As atoms in the first As layer above the first In layer in the 124 and 407 Å nanomesas. The vertical displacement is measured with respect to a reference position of $z=314$ Å. In order to show the details of the morphology of the layer, the vertical displacement of each atom has been magnified by a factor of 40. For the 124 Å nanomesa shown in Fig. 13(a), the As layer is “dome” shaped, in which atoms have an upward displacement of ~ 0.8 Å at the center and a downward displacement of ~ 0.5 Å at the edges. In contrast, the As layer in the 407 Å nanomesa shows a “dimple” at the center of the mesa, see Fig. 13(b). At the “rim” and “bottom” of the dimple, atoms have upward displacements of ~ 1.0 and ~ 0.5 Å, respectively, while atoms at the edges have a downward displacement of ~ 1.6 Å. The dimple is located at roughly the same position as the enhanced compressive stress domain shown in Fig. 12(b). The morphology of the nanomesa, de-

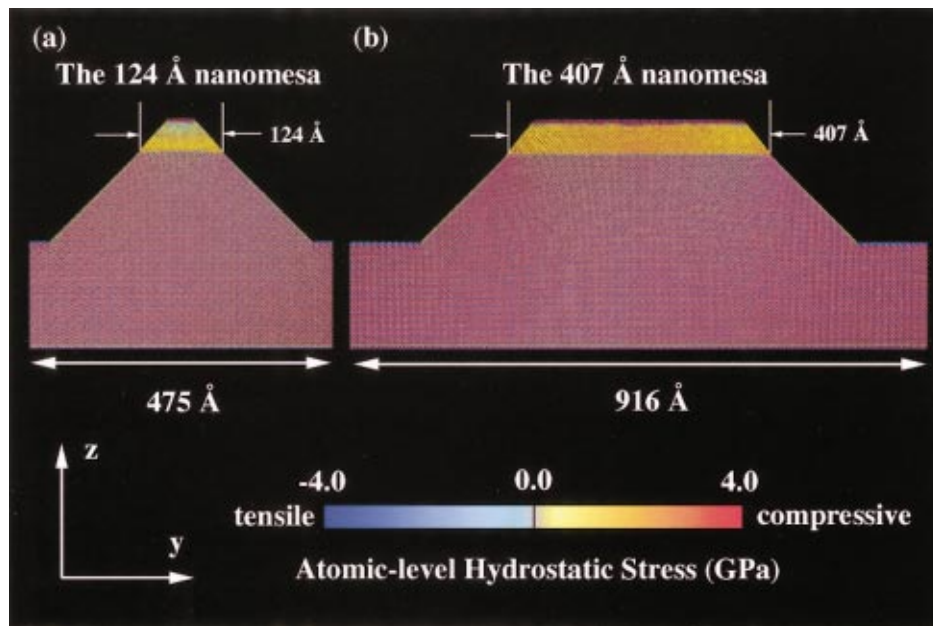


FIG. 12. (Color) Atomic-level hydrostatic stress in the cross sections through the center of the (a) 124 Å, and (b) 407 Å nanomesas.

scribed by the vertical displacements of As atoms in the first As layer above the first In layer, together with the stress distribution in the nanomesa, which is evidenced by the stress domains in the InAs overlayers, largely determine the energetic state of the nanomesa. In the 124 Å nanomesa shown in Fig. 13(a), the morphology of the As layer is regular and smooth, and the hydrostatic stress in the InAs overlayer is homogeneous (containing only one domain). In the 407 Å nanomesa shown in Fig. 13(b), however, the morphology of the As layer is irregular and rough, and the hydrostatic stress in the InAs overlayer is inhomogeneous (containing multiple domains). This provides clear evidence that there exists a critical lateral size for such stress domain formation. It is found that the morphology of the As layer in

Fig. 13(b) is a superposition of four domes whose sizes are estimated to be ~30 nm. The existence of such stress domains is consistent with the experimental findings for the deposition of InAs on GaAs stripe mesa tops:¹⁴ the number of parallel chains of InAs islands varies from 3 to 1 as the stripe width goes from 100 to 30 nm, i.e., in multiples of ~30 nm of GaAs mesa lateral sizes.

The structural correlations in the InAs/GaAs nanomesas are analyzed by calculating the pair distribution function (PDF), $g(r)$, which gives the probability of finding a pair of atoms a distance r apart, relative to the probability for a completely random distribution at the same density. Figure 14(a) shows the In–In and In–As PDFs that are averaged over the whole 124 Å nanomesa. The In–In and In–As PDFs

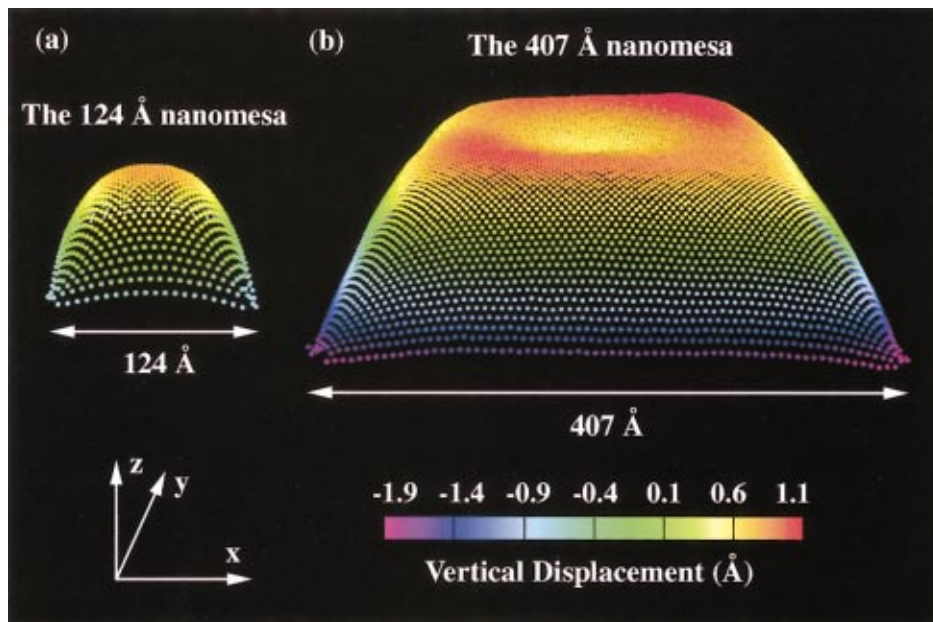


FIG. 13. (Color) Vertical displacement of As atoms in the first As layer above the first In layer in the (a) 124 Å, and (b) 407 Å nanomesas.

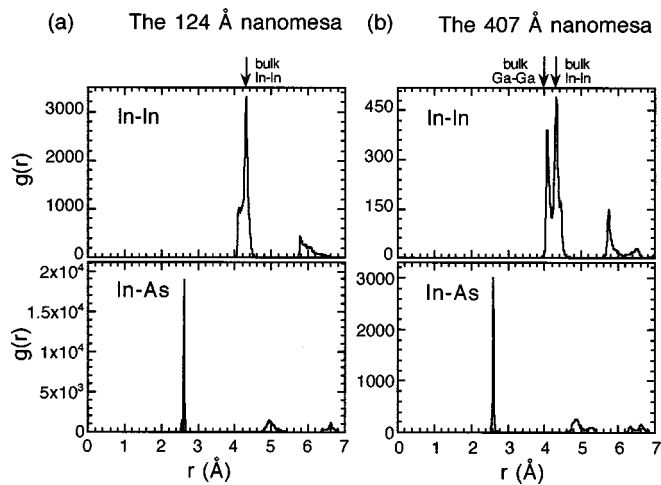


FIG. 14. In–In and In–As pair distribution functions in the (a) 124 Å, and (b) 407 Å nanomesas.

averaged over the whole 407 Å nanomesa are shown in Fig. 14(b). For the 124 Å nanomesa, the In–In PDF has only one first-neighbor peak at 4.30 Å (which is slightly larger than the InAs bulk value, 4.28 Å); see Fig. 14(a). This suggests that the lattice spacing in the InAs overlayer is mostly relaxed to its bulk value. For the 407 Å nanomesa, however, the first-neighbor peak of the In–In PDF is split into two subpeaks: 4.06 and 4.31 Å; see Fig. 14(b). The 4.06 Å subpeak is close to the GaAs bulk value, 4.00 Å, and the 4.31 Å subpeak is slightly larger than the InAs bulk value, 4.28 Å. On the other hand, the In–As PDFs in the two nanomesas show that the first-neighbor peak positions are essentially the same as the InAs bulk value.

In order to understand the origin of the split first-neighbor peak in In–In PDF in the 407 Å nanomesa, we calculate the in-plane [i.e., parallel to the InAs/GaAs(001) interface] In–In PDF that is averaged over each InAs layer.

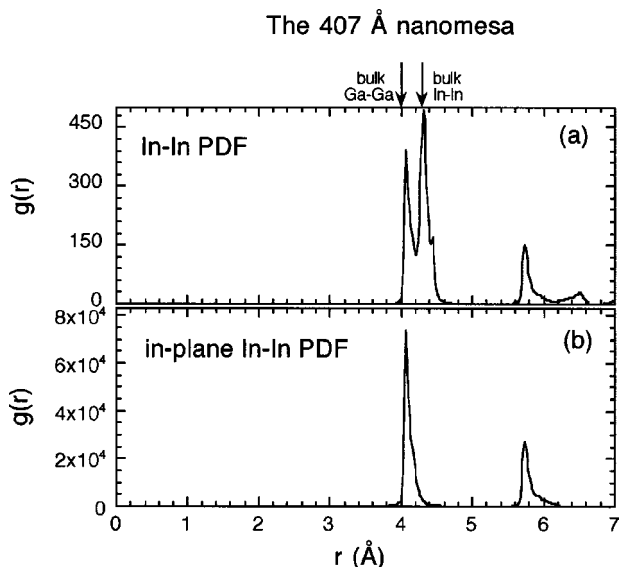


FIG. 15. (a) In–In pair distribution function and (b) the in-plane In–In pair distribution function of InAs layer parallel to the InAs/GaAs(001) interface, in the 12 ML InAs overlayer of the 407 Å nanomesa.

Figure 15(a) shows the In–In PDF that is averaged over the whole 407 Å nanomesa. The sum of the in-plane In–In PDFs in each InAs layer is shown in Fig. 15(b). It can be seen that the first subpeak in Fig. 15(a) coincides with the first peak in Fig. 15(b). This shows that the first subpeak of the In–In PDF is entirely due to in-plane correlations in each InAs layer. On the other hand, the second subpeak in the In–In PDF is due to the interplane correlations in the 407 Å nanomesa. In other words, the InAs overlayer is laterally constrained to the GaAs lattice near the interface but vertically relaxed to a value that exceeds the InAs lattice.

VII. SUMMARY

We have developed model potentials for GaAs(100) and InAs(100) surface atoms. Surface energies of GaAs and InAs for the (100), (110), and (111) orientations have been calculated. Both MD and the CG method are used and the results are in excellent agreement. Surface reconstructions on GaAs(100) and InAs(100) are studied via the CG method. Not only do these model potentials reproduce well the surface energies for the (100) orientation, these also yield (1×2) dimer lengths in accordance with *ab initio* calculations.

We have performed large-scale MD simulations of InAs/GaAs square nanomesas with {101}-type sidewalls. Qualitatively, the effect of lattice mismatch can be isolated by studying GaAs square nanomesas of exactly the same geometry as the InAs/GaAs nanomesas, with the InAs overlayers replaced by GaAs overlayers. After isolating the effect of lattice mismatch, it is found that the InAs in-plane lattice constant starts to exceed the InAs bulk value at 12 ML. Moreover, the hydrostatic stresses in InAs layers are tensile above \sim twelfth monolayer, in contrast to the compressive stresses in the InAs layers below \sim twelfth monolayer. Therefore, it is not energetically favorable to have InAs overlayers thicker than 12 ML.

We have also performed multimillion-atom molecular dynamics simulations of InAs/GaAs square nanomesas with {101}-type sidewalls to investigate the lateral size effect on the stress distribution and morphology. The simulations indicate the existence of a critical lateral size for stress domain formation in accordance with recent experimental findings. A single stress domain is found in small (≤ 40 nm) mesa, whereas a larger mesa contains two stress domains. It is also found that, in the larger nanomesa, the InAs overlayer is laterally constrained to the GaAs bulk near the interface but vertically relaxed to slightly above the InAs bulk.

ACKNOWLEDGMENTS

This work was supported by AFOSR under the USC–LSU Multidisciplinary University Research Initiative, and by NSF, DOE, and NASA. The authors thank Dr. M. A. Makeev for critical reading of the manuscript and useful discussions. Simulations were performed using the 64-processor Digital Alpha and the 166-node PC cluster in the Concurrent Computing Laboratory for Materials Simulations at Louisiana State University and parallel computers at DOD's Major Shared Resource Centers under a DOD Challenge Project.

- ¹G. Göthelid, Y. Garreau, M. Sauvage-Simkin, R. Pinchaux, A. Cricenti, and G. Le Lay, *Phys. Rev. B* **59**, 15285 (1999).
- ²V. P. LaBella, H. Yang, D. W. Bullock, and P. M. Thibado, *Phys. Rev. Lett.* **83**, 2989 (1999).
- ³T. Hashizume, Q. K. Xue, J. Zhou, A. Ichimiya, and T. Sakurai, *Phys. Rev. Lett.* **73**, 2208 (1994).
- ⁴G. R. Bell, J. G. Belk, C. F. McConville, and T. S. Jones, *Phys. Rev. B* **59**, 2947 (1999).
- ⁵G. P. Srivastava and S. J. Jenkins, *Phys. Rev. B* **53**, 12589 (1996).
- ⁶H. Yamaguchi and Y. Horikoshi, *Phys. Rev. B* **51**, 9836 (1999).
- ⁷Q. Xue, T. Ogino, H. Kiyama, Y. Hasegawa, T. Sakurai, *J. Cryst. Growth* **175/176**, 174 (1997).
- ⁸S. Guha, A. Madhukar, and K. C. Rajkumar, *Appl. Phys. Lett.* **57**, 2110 (1990).
- ⁹Q. Xie, A. Madhukar, and P. Chen, *Appl. Phys. Lett.* **65**, 2051 (1994).
- ¹⁰Q. Xie, P. Chen, A. Kalburge, T. R. Ramachandran, A. Nayfonov, A. Konkar, and A. Madhukar, *J. Cryst. Growth* **150**, 357 (1995).
- ¹¹Q. Xie, A. Madhukar, P. Chen, and N. P. Kobayashi, *Phys. Rev. Lett.* **75**, 2542 (1995).
- ¹²A. Konkar, K. C. Rajkumar, Q. Xie, P. Chen, A. Madhukar, H. T. Lin, and D. H. Rich, *J. Cryst. Growth* **150**, 311 (1995).
- ¹³A. Konkar, A. Madhukar, and P. Chen, *Mater. Res. Soc. Symp. Proc.* **380**, 17 (1995).
- ¹⁴A. Konkar, A. Madhukar, and P. Chen, *Appl. Phys. Lett.* **72**, 220 (1998).
- ¹⁵D. Bimberg, M. Grundmann, and N. N. Ledentsov, *Quantum Dot Heterostructures* (Wiley, London, U.K., 1998).
- ¹⁶R. L. Sellin, I. Kaiander, D. Ouyang, T. Kettler, V. W. Pohl, D. Bimberg, N. D. Zakharov, and P. Werner, *Appl. Phys. Lett.* **82**, 841 (2003).
- ¹⁷A. R. Kovsh, N. A. Maleev, A. E. Zhukov, S. S. Mikhlin, A. P. Vasil'ev, Y. M. Shernyakov, M. V. Maximov, D. A. Livshits, V. M. Ustinov, Z. L. Alferoy, N. N. Ledentsov, D. Bimberg, *Electron. Lett.* **38**, 1104 (2002).
- ¹⁸M. Grundmann, O. Stier, and D. Bimberg, *Phys. Rev. B* **52**, 11969 (1995).
- ¹⁹O. Stier, M. Grundmann, and D. Bimberg, *Phys. Rev. B* **59**, 5688 (1999), and references therein.
- ²⁰A. J. Williamson, L. W. Wang, and A. Zunger, *Phys. Rev. B* **62**, 12963 (2000), and references therein.
- ²¹S. J. Sun and Y. C. Chang, *Phys. Rev. B* **62**, 13631 (2000).
- ²²H. Jiang and J. Singh, *Phys. Rev. B* **56**, 4696 (1997).
- ²³C. Pryor, J. Kim, L. W. Wang, A. J. Williamson, and A. Zunger, *J. Appl. Phys.* **83**, 2548 (1998).
- ²⁴M. A. Makeev and A. Madhukar, *Phys. Rev. Lett.* **86**, 5542 (2001).
- ²⁵G. S. Pearson and D. A. Faux, *J. Appl. Phys.* **88**, 730 (2000).
- ²⁶W. Yu and A. Madhukar, in *Proceedings of the 23rd ICPS Conference, Berlin, July 1996*, edited by M. Scheffler and R. Zimmerman (World Scientific, Singapore, 1996), p. 1309.
- ²⁷W. H. Duan, R. M. Wentzcovitch, and J. R. Chelikowsky, *Phys. Rev. B* **60**, 3751 (1999).
- ²⁸V. I. Pipa, V. V. Mitin, and M. Stroschio, *Appl. Phys. Lett.* **74**, 1585 (1999).
- ²⁹O. Shenderova, D. W. Brenner, A. Nazarov, A. Romanov, and L. Yang, *Phys. Rev. B* **57**, R3181 (1998).
- ³⁰D. G. Truhlar and V. Mckoy, *Comput. Sci. Eng.* **2**, 19 (2000).
- ³¹N. Binggeli and J. R. Chelikowsky, *Phys. Rev. Lett.* **75**, 493 (1995).
- ³²M. Z. Bazant, E. Kaxiras, and J. F. Justo, *Phys. Rev. B* **56**, 8542 (1997).
- ³³D. W. Brenner, *Phys. Status Solidi B* **217**, 23 (2000).
- ³⁴D. Srivastava, M. Menon, and K. Cho, *Phys. Rev. Lett.* **83**, 2973 (1999).
- ³⁵W. Yu and A. Madhukar, *Phys. Rev. Lett.* **79**, 905 (1997); **79**, 4939 (1997).
- ³⁶N. Moll, A. Kley, E. Pehlke, and M. Scheffler, *Phys. Rev. B* **54**, 8844 (1996).
- ³⁷E. Pehlke, N. Moll, A. Kley, and M. Scheffler, *Appl. Phys. A: Mater. Sci. Process.* **65**, 525 (1997).
- ³⁸G.-X. Qian, R. M. Martin, and D. J. Chadi, *Phys. Rev. B* **38**, 7649 (1988).
- ³⁹F. H. Stillinger and T. A. Weber, *Phys. Rev. B* **31**, 5262 (1985).
- ⁴⁰P. Vashishta, R. K. Kalia, A. Nakano, W. Li, and I. Ebbsjö, *NATO ASI* **3/23**, 151 (1997).
- ⁴¹I. Ebbsjö, R. K. Kalia, A. Nakano, J. P. Rino, and P. Vashishta, *J. Appl. Phys.* **87**, 7708 (2000).
- ⁴²S. Kodiyalam, R. K. Kalia, H. Kikuchi, A. Nakano, F. Shimojo, and P. Vashishta, *Phys. Rev. Lett.* **86**, 55 (2001).
- ⁴³P. S. Branicio, R. K. Kalia, A. Nakano, and P. Vashishta (unpublished).
- ⁴⁴X. Su, R. K. Kalia, A. Nakano, P. Vashishta, and A. Madhukar, *Appl. Phys. Lett.* **78**, 3717 (2001); **79**, 4577 (2001).
- ⁴⁵The convergence with respect to the thickness of the slab supercell in the z direction is tested by performing another simulation in which the thickness is doubled, with all the other dimensions fixed. The surface energy in this case differs $\sim 0.1\%$, suggesting that 5 unit cells in the z direction is sufficient thickness for converged results.
- ⁴⁶M. Tuckerman, B. J. Berne, and G. J. Martyna, *J. Chem. Phys.* **97**, 1990 (1992).
- ⁴⁷C. Messmer and J. C. Bilello, *J. Appl. Phys.* **52**, 4623 (1981).
- ⁴⁸L. A. Zepeda-Ruiz, D. Maroudas, and W. H. Weinberg, *J. Appl. Phys.* **85**, 3677 (1999).
- ⁴⁹E. Lidorikis, M. E. Bachlechner, R. K. Kalia, A. Nakano, P. Vashishta, and G. Z. Voyiadjis, *Phys. Rev. Lett.* **87**, 086104 (2001).
- ⁵⁰S. Ogata, E. Lidorikis, F. Shimojo, A. Nakano, P. Vashishta, and R. K. Kalia, *Comput. Phys. Commun.* **138**, 143 (2001).